Direct Force Measurements between TiO$_2$ Surfaces

Ian Larson,[†] Calum J. Drummond,*,‡ Derek Y. C. Chan,[§] and Franz Grieser*,[†]

Contribution from the Advanced Mineral Products Research Centre, School of Chemistry and Department of Mathematics, University of Melbourne, Parkville, Victoria 3052, Australia, and CSIRO Division of Chemicals and Polymers, Private Bag 10, Rosebank MDC, Clayton, Victoria 3169, Australia

Received June 11, 1993[®]

Abstract: An atomic force microscope (AFM) has been used to measure the force of interaction between a rutile titanium dioxide colloid and a single macroscopic rutile crystal in aqueous solution. The effect of pH and electrolyte concentration on the force has been investigated. ζ potentials were derived from electrophoretic mobility measurements on the rutile colloid as a function of pH and electrolyte concentration. Experimental decay lengths for the repulsive electrical double layer interaction are in good agreement with the theoretical Debye lengths at $<10^{-2}$ M electrolyte. Measurements at the isoelectric point, i.e. pH = 5.6 of the TiO$_2$, could be fitted with a nonretarded Hamaker constant of $6 \pm 2\ 10^{-20}$ J. This value agrees well with the van der Waals interaction calculated within the framework of the Lifshitz theory. In the calculation we used the Ninham–Parsegian representation for the dielectric susceptibility function and have utilized refractive index versus wavelength data to characterize the van der Waals interaction in rutile systems. A non-retarded Hamaker constant of $7 \pm 1 \times 10^{-20}$ J was calculated for two rutile surfaces interacting across water.

Introduction

A technique has recently been developed using an atomic force microscope (AFM) that allows the measurement of the force distance relationship between a colloidal particle and a macroscopic flat surface with sub-nanometer separation and sub-nano-Newton force resolution.[1–6] Even more recently the AFM has been used to measure the interaction between two colloidal particles.[7] The AFM method basically uses the deflection of a spring cantilever to which a colloidal particle is attached to measure a direct interaction force as a function of the displacement of the flat surface toward the cantilever.

At present there are very few techniques that can be used to measure the forces between macroscopic bodies at these small separations with this level of accuracy;[8–11] the most common utilizes the surface force apparatus, (SFA).[10] The AFM and SFA techniques are complementary with both having comparative advantages and disadvantages. The main advantages of the AFM are associated with the speed of measurement and the variety of materials that can be used in the measurements.

In the present study the forces between a rutile titanium dioxide colloidal sphere and a rutile titanium dioxide single crystal, a flat plate, have been measured as a function of pH and electrolyte concentration. Theoretical calculations of the nonretarded Hamaker constant[12] and electrophoretic mobility measurements on the TiO$_2$ colloids have also been performed to allow a thorough evaluation of the results obtained from the AFM technique.

TiO$_2$ was chosen because of its fundamental relevance in many industrial and medical applications[13–15] and its relatively high Hamaker constant.

Theory

According to the theory of colloidal stability of Derjaguin–Landau–Verwey–Overbeek[16] (DLVO), the interaction between identically charged colloidal particles can be separated into two contributions: an attractive van der Waals interaction and a repulsive electrostatic force. The total interaction free energy is taken as a sum of these two terms.

The physical dimensions of the surfaces allow the use of the Derjaguin approximation[17] to relate the force (F) between the sphere, radius (R), and the flat plate in terms of the interaction free energy per unit area between parallel plates of the same material. In the Derjaguin approximation the force F between the sphere and plate has the form

$$F/R = 2\pi(V_A + V_R) \tag{1}$$

where V_A is the attractive van der Waals interaction free energy per unit area and V_R is the electric double layer interaction free energy per unit area between two flat plates of the same material. For simplicity we ignore the effect of retardation[18] on the van der Waals force so we have

$$V_A = -A_H/12\pi H^2 \tag{2}$$

where A_H is the Hamaker constant and H is the distance of closest approach between the sphere and the plate.

To calculate the repulsive double layer interaction, V_R in eq 1, for the constant charge or constant potential limits of the

* Authors to whom correspondence should be addressed.
† School of Chemistry, University of Melbourne.
‡ CSIRO Division of Chemicals and Polymers.
§ Department of Mathematics, University of Melbourne.
® Abstract published in *Advance ACS Abstracts,* November 15, 1993.
(1) Ducker, W. A.; Senden, T. J.; Pashley, R. M. *Nature* 1991, *353*, 239.
(2) Butt, H-J. *Biophys. J.* 1991, *60*, 1438.
(3) Ducker, W. A.; Senden, T. J.; Pashley, R. M. *Langmuir* 1992, *8*, 1831.
(4) Meagher, L. *J. Colloid Interface Sci.* 1992, *152*, 293.
(5) Rutland, M. W.; Senden, T. J. *Langmuir* 1993, *9*, 412.
(6) Drummond, C. J.; Senden T. J. Submitted for publication.
(7) Li, Y. Q.; Tao, N. J.; Garcia, A. A.; Lindsay, S. M. *Langmuir* 1993, *9*, 637.
(8) LeNeveu, D. M.; Rand, R. P.; Parsegan, V. A. *Nature* 1976, *259*, 601.
(9) Derjaguin, B. V.; Rabinovich, Y. I.; Churev, N. V. *Nature* 1978, *272*, 313.
(10) Israelachvili, J. N.; Adams, G. *J. Chem. Soc., Faraday Trans 1* 1978, *74*, 975.
(11) Lorenz, D.; Adamczyk, Z.; Belouschek, P. *Colloids Surf.* 1991, *57*, 355.
(12) Hamaker, H. C. *Physics* 1937, *4*, 1058.

(13) *Kirk-Othmer Encyclopaedia of Chemical Technology,* 3rd ed.; Wiley: New York, 1983; Vols. 17 and 23.
(14) Li, J. *Biomaterials* 1993, *14*, 229.
(15) Oshida, Y.; Sachdeva, R.; Miyazaki, S. *J. Mater. Sci. Mater. Med.* 1992, *3*, 306.
(16) Derjaguin, B. V.; Landau, L. *Acta Physiochem.* 1941, *14*, 633. Verwey, E. G. W.; Overbeek, J. T. G. *The Theory of the Stability of Lyophobic Colloids*; Elsevier: Amsterdam, 1948.
(17) Derjaguin, B. V. *Kolloid-Z* 1934, *69*, 155.
(18) Most colloid and surface science texts will present a section on this. A very good account is given by Hunter, R. J. *Foundations of Colloid Science*; Oxford University Press: Oxford, 1989; Vol. I, p 188.
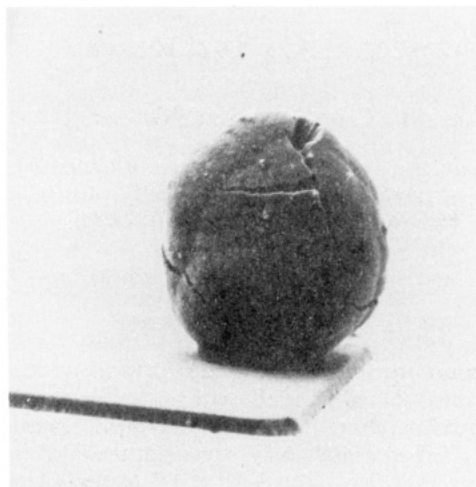
Figure 1. SEM micrograph of a colloid probe used in this study. The surface roughness is typical of this sample of TiO_2 colloidal material.

nonlinearized Poisson–Boltzmann equation, we use the method described by Chan et al.[19]

Experimental Section

TiO_2 Colloids. The sample of colloidal TiO_2 was obtained from Tioxide Chemicals Ltd., UK, and consisted of approximately 9 μm diameter spheres. The TiO_2 was made by the hydrolysis of $TiCl_4$. The process used to synthesize these colloids resulted in fissures occurring in approximately 50% of the sample. These fissures, combined with the inherent surface roughness of the colloids, made it difficult to determine the local radius of curvature. The sample was soxhlet washed for 72 h with the water changed every 12 h to remove any traces of residual chloride. Electron spectroscopy for chemical analysis (ESCA) performed on the cleaned powder showed only titanium, oxygen, and adventitious carbon to be present. There was no indication of the presence of any chlorine or any other element. X-ray diffraction showed that the titanium oxide was 100% rutile.

Colloid Probe Preparation. The method of preparing the colloidal sphere for force measurements has been described elsewhere.[1,3,6] In brief, the colloidal particle is glued to a microfabricated AFM silicon nitride cantilever with a low melting point inert wax (Shell Epikote Resin 1002). This assembly will be referred to as a colloid probe. In Figure 1 we show a micrograph of a colloid probe used in these experiments obtained by scanning electron microscopy (SEM). The cantilevers (Park Scientific, Mountain View, CA) did not have pyramidal tips. Cantilevers without tips were used so that there could be no doubt that it was the colloid particle, and not the pyramidal tip, that was interacting with the flat surface. The one variation to the method described in ref 1 was that the probes were not exposed to a water plasma as part of the cleaning procedure. The probes were rinsed with AR grade ethanol and blown dry with nitrogen immediately before use.

TiO_2 Crystal. The rutile TiO_2 single crystal was obtained from British Titan Products, England. The crystal was polished to optical smoothness, and AFM images of the surface showed that the RMS roughness was approximately 3 nm over 10 μm^2. The crystal was soaked in 10^{-3} M HNO_3 overnight and then steamed cleaned for 5 h before use to remove any surface contamination. ESCA experiments indicated that there was less than 1% tin or lead present. X-ray diffraction confirmed that the crystal was rutile in structure. As with the probes, the crystal was rinsed with ethanol and blown dry immediately before use.

Reagents. Analytical grade KNO_3, KOH, and HNO_3 were used without further purification. High grade nitrogen (99%) and AJAX AR grade ethanol were used as supplied by the commercial supplier. Millipore "Milli-Q" water was used throughout.

Force Measurements. The measurements were made on a Digital Instruments, Inc. (Santa Barbara, CA) Nanoscope III atomic force microscope. The technique used to make these measurements has been described elsewhere.[1,3,6] The Nanoscope III has a "Force" mode in which the colloid probe is held stationary and the single-crystal, flat surface, mounted on a piezoelectric ceramic tube, can be driven in a controlled

manner toward and away from the colloidal probe. This takes place in an aqueous electrolytic environment which can be changed via a syringe or a peristaltic pump connected to an external reservoir.

To monitor the cantilever deflection a laser beam is reflected off the back of the cantilever onto a split photodiode. The software of the Nanoscope generates a file that contains the output of the photodiode and the displacement of the sample. These raw data are then converted into force versus separation. First, zero force and zero separation need to be defined. Zero force was determined at large probe–crystal separations where the colloid probe position did not change with a change in position of the crystal. Zero separation was defined as when a change in the crystal position caused an equal change in the cantilever deflection. In this region of compliance the output of the photodiode is a linear function of the displacement of the crystal. Hooke's law was then used to convert the change in cantilever position to absolute force and the displacement data were converted to separation.

A technique developed by Senden and Ducker[20] was used to experimentally determine the spring constants of the cantilevers used. A large tungsten sphere (radius $\sim$ 20 μm, supplied by GTE Sylvania, Towanda, PA) was attached to a cantilever in the same way as described earlier in making the colloid probes. The deflection of the cantilever due to the weight of the tungsten sphere was measured. This is easily done by recording the output of the photodiode with the cantilever hanging freely and, after inverting the head of the AFM so that the cantilever is hanging upside down, recording the output again. The difference, X, is equal to twice the deflection due to gravity. This procedure was repeated many times in order to obtain an average value of X. It is important to note that the voltage displayed on the digital voltage meter is different from that saved by the computer; it is therefore necessary to use the values stored by the computer and not the digital meter reading.

By measuring a force curve between the tungsten sphere and a hard metal surface, the gradient of the compliance region, Ω, allowed the photodiode output to be converted to an actual deflection distance. By measuring the radius of the sphere, R, and knowing the density of tungsten, ρ, the spring constant of the cantilever, k, could be calculated by equating Hooke's law, $F = kx$, to Newton's second law, $F = mg$, where m is the mass of the tungsten sphere, giving

$$k = 8\pi R^3 \rho g / 3\Omega X \qquad (3)$$

We used rectangular single beam cantilevers with a measured spring constant of 0.26 ± 0.04 N/m. This is an average value based on the measurement of 5 cantilevers. This value is somewhat larger than the value quoted by the manufacturer, $k = 0.16$ N/m. Our larger value is most likely due to the cantilevers used being slightly thicker than quoted by the manufacturer and the silicon nitride cantilever material having a different Young's modulus than used in the manufacturer's calculations.

Errors in Force Measurements. Vibrational, thermal, and electronic noise during the experiments was approximately ±0.02 nN.

To accurately calculate the separation between the two surfaces a knowledge of the response of the piezoelectric ceramic tube to applied voltage is required. The manufacturer's calibration was checked by measuring the height of the tracks on a CD stamper with the AFM; these tracks have been previously characterized by ellipsometry. The manufacturer's piezocalibration was found to be correct to within $\pm$ 5%.

The spring constants for the cantilevers used could only be determined to within $\pm15\%$.

The total error in the force measurements is approximately $\pm20\%$.

Electrophoresis Measurements. A Rank Bros. Mk. II instrument was used to measure the electrophoretic velocity, v_E, as a function of pH. For the large particle size used in our experiments, the zeta-potentials, ζ, of the particles can be calculated from these velocities by the Helmholtz–Smoluchowski equation[21]

$$\zeta = v_E \eta / E\epsilon \qquad (4)$$

where η is the viscosity of the medium, E the electric field strength, and ϵ the permittivity of the electrolyte medium. Electrophoretic velocities were measured at 25 °C.

Results and Discussion

(i) Electrophoresis Measurements. The electrophoretically determined iep of the colloidal TiO_2 was found to be pH 5.6 $\pm$ 0.2, which agrees well with literature values for pure, uncon-

(19) Chan, D. Y. C.; Pashley, R. M.; White, L. R. *J. Colloid Interface Sci.* **1980**, *77*, 283.

(20) Senden, T. J. Personal communication.
(21) The form of the equation shown is in SI units.

Direct Force Measurements between TiO$_2$ Surfaces

J. Am. Chem. Soc., Vol. 115, No. 25, 1993 11887
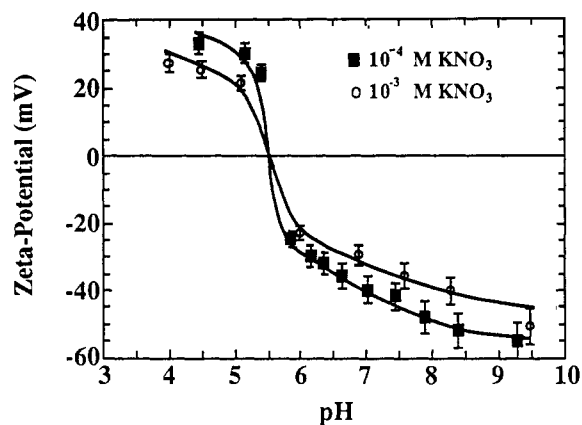
Figure 2. Electrophoretically determined ζ-potentials of the TiO$_2$ colloid as a function of pH and electrolyte concentration. Within experimental error the iep in both experiments is pH 5.6 $\pm$ 0.2.

taminated, and "aged" rutile[22-25] and corresponds extremely well with the pH at which the force–separation curves show only an attractive component. Electrolyte concentrations of 10^{-4} and 10^{-3} M KNO$_3$ were used as these were the concentrations used in the majority of force measurements. The ζ-potential curves obtained from electrophoretic mobility measurements over a range of pH are shown in Figure 2. KNO$_3$ was chosen as the electrolyte because it has been reported as being an indifferent electrolyte for TiO$_2$.[26-28]

(ii) Force measurements. The surface roughness of the colloid probes made it very difficult to determine the colloid radii definitively. The extent of surface roughness can be clearly seen in the example shown in Figure 1. As all the experimental data are scaled by the radius of curvature of the colloid probe interacting with the polished TiO$_2$ crystal, it is necessary to know the effective radius accurately. To do this we determined an effective probe radius by assuming that the ζ potential was equal to the diffuse layer potential[25] under high pH and low salt conditions. In Figure 3a we show the fit for the colloid probe shown in Figure 1 with an effective radius of 8.4 μm. The ζ potential at pH 9.3, with 10^{-4} M KNO$_3$ present, was 55 mV. The effective probe radius was determined by fitting the experimental force data to solutions of the nonlinearized Poisson–Boltzmann equation with $\Psi_d = 55$ mV. This unique effective radius was then used to scale the rest of the experimental data taken with that probe. For example, in Figure 3b we show the normalized force–separation curve with 10^{-4} M KNO$_3$ at pH 7.2. An effective radius was similarly determined for each probe used. Surface roughness considerations become important when the extent of the surface force approaches the magnitude of the surface roughness. For this reason we have primarily focussed our attention on force measurements conducted in low electrolyte, large Debye-length solutions. It is worth noting that any error in the spring constant measurement is nullified by determining an effective probe radius because the experimental force data are scaled by k/R.

The total force, eq 1, has been calculated under the assumption of constant diffuse layer potential or constant diffuse-layer charge boundary conditions as described earlier. These two models represent the lower and upper limits for the double layer interaction. At large separations there is little difference between the two boundary conditions: the data fit both models equally

Figure 3. (a, top) Force–separation curve scaled to fit theory curves under the assumption that the diffuse-layer potential equals the ζ-potential under these conditions. The upper fitted curve is the constant charge limit and the lower curve is the constant potential curve. The fitting parameters are the following: potential $= -55$ mV and Debye length $= 25$ nm. The background electrolyte concentration was 1.0×10^{-4} M KNO$_3$. From this fit the effective colloid probe radius is determined. This effective radius is then used to normalize all the experimental data taken with this probe. (b, bottom) Force–separation curve taken at pH 7.2. The fitted curves are as in part a. The fitting parameters are the following: potential $= -38$ mV and Debye length $= 10$ nm. The background electrolyte concentration was 1.0×10^{-4} M KNO$_3$. The effective radius determined in part a was used to normalize the data.

well. It is not until the separation becomes relatively small that the difference between the two limits becomes appreciable; in this region the experimental data lie between these two limits. This is essentially the same behavior as has been reported for SiO$_2$.[1,29,30] A variety of models have been developed to explain this behavior which is also seen in electrochemical measurements. These models describe the relationship between surface charge and potential, and the solution in terms of surface site density, ionization constants, pH, and electrolyte concentration.[25,31]

To calculate the double layer interaction, at constant potential or constant charge, it is necessary to know the value of the diffuse layer potential when the surfaces are far apart. The value of this diffuse layer potential is chosen to fit the experimental force separation curve at large separations, with the exception of pH 9.3 and 10^{-4} M KNO$_3$ where it is assumed to be 55 mV.

In deriving the diffuse-layer potentials from the force–separation curves it has been assumed that the diffuse layer

(22) James, R. O.; Healy, T. W. *J. Colloid Interface Sci.* **1972**, *40*, 53.

(23) Healy, T. W.; Wiese, G. R.; Yates, D. E.; Kavanagh, B. V. *J. Colloid Interface Sci.* **1973**, *42*, 647.
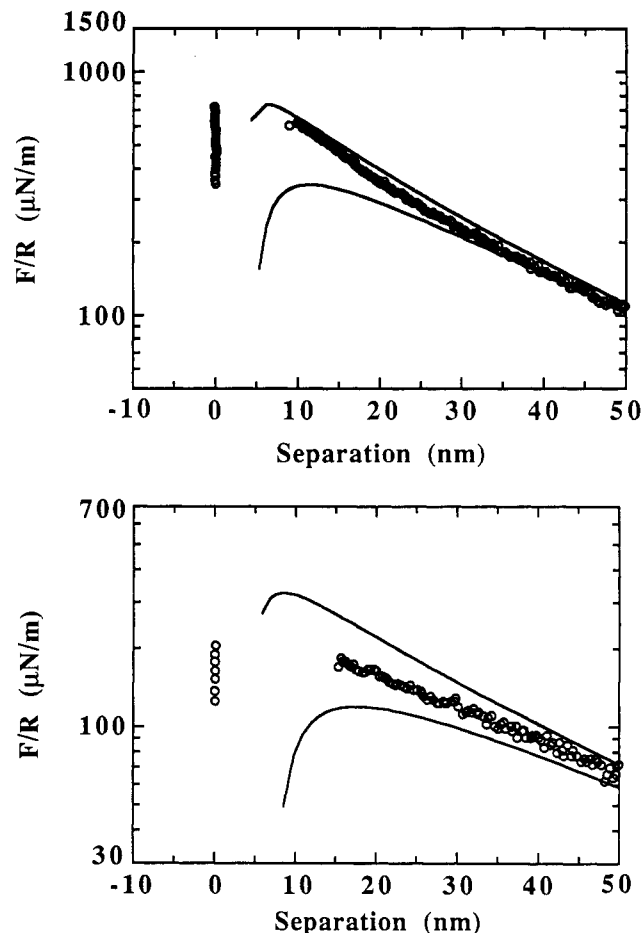
(24) Wiese, G. R.; Healy, T. W. *J. Colloid Interface Sci.* **1975**, *51*, 567.

(25) Hunter, R. J. *Zeta Potential in Colloid Science*, Academic: London, 1988; p342.

(26) Parfitt, G. D.; Ramsbotham, J.; Rochester, C. H. *J. Colloid Interface Sci.* **1972**, *41*, 437.

(27) Smith, A. L. *J. Colloid Interface Sci.* **1976**, *55*, 525.

(28) Furlong, D. N.; Parfitt, G. D. *J. Colloid Interface Sci.* **1978**, *65*, 548.

(29) Peschel, G.; Belouschek, R.; Müller, M. M.; Müller, M. R.; Konig, R. *Colloid Polym. Sci.* **1982**, *260*, 444.

(30) Horn, R. G.; Smith, D. T.; Haller, W. *Chem. Phys. Lett.* **1989**, *162*, 404.

(31) A good review of these models, inculding examples for TiO$_2$, is given by; James, R. O. *Adv. Ceram.* Ceramic **1985**, *21*, 1ff.
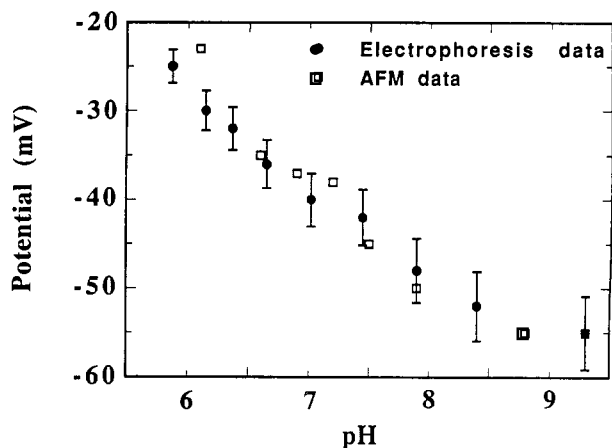
Figure 4. Comparison between potentials determined by AFM force measurements and electrophoretic measurements. A background electrolyte of 1.0×10^{-4} M KNO_3 was present in both experiments. The diffuse-layer potential is assumed to be equal to the ζ-potential at pH 9.3. The other diffuse-layer potentials are obtained by using the effective radius determined by equating the two potentials.
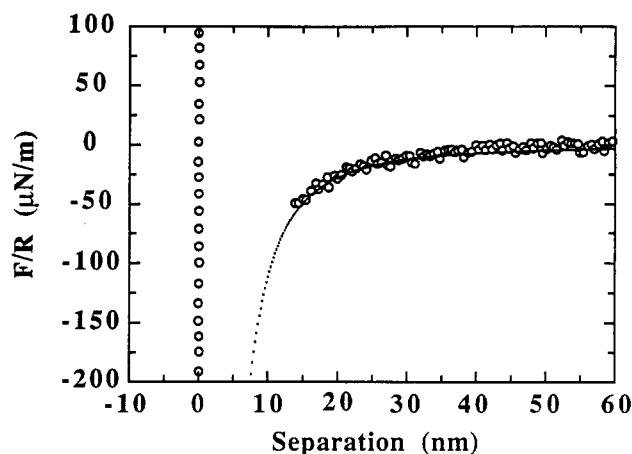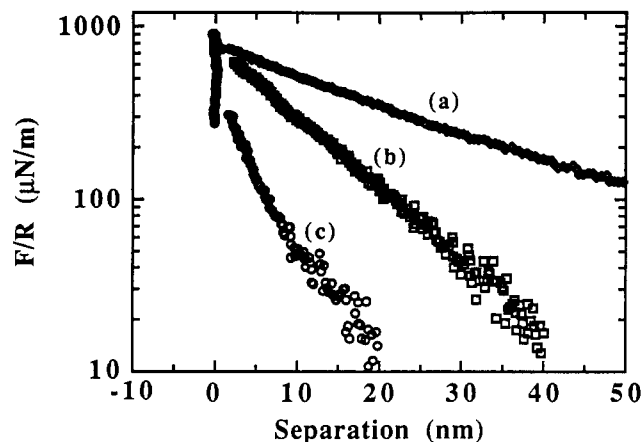

Figure 5. Force–separation curve taken at the iep of the TiO_2 used in this study. The force–separation points have been scaled by the effective radius of the colloid probe. The full curve is the theoretical interaction using the non-retarded Hamaker constant calculated from Lifshitz theory. The background electrolyte concentration was 1.0×10^{-4} M KNO_3.

commences at the "hard wall" contact, as ascertained from the linear compliance part of the cantilever deflection curve. Incorporation of a Stern layer[32,33] would result in a very slight reduction in the magnitude of the calculated potential (still within experimental error bounds) in 10^{-4} M KNO_3.

A surface charge reversal has been observed at low pH values although not consistently. This low pH region is currently being studied in detail.

A comparison of the ζ-potentials and the scaled diffuse-layer potentials, measured by electrophoresis and force measurements, respectively, is shown in Figure 4. There is very good agreement between the potentials measured by the two techniques at low and medium potentials.

The force versus separation curve taken at a pH of 5.6 shown in Figure 5 is at the pH corresponding to the isoelectric point (iep) of the material and hence there is no electrostatic interaction between the TiO_2 surfaces. The force–separation curve is essentially due to the van der Waals interaction between the sphere and the flat surface. A non-retarded Hamaker constant of $6 \pm 2 \times 10^{-20}$ J fits the experimental data; the error is due to the error in the ζ-potential measurement of 55 mV. This is the first direct measurement of the van der Waals interaction between rutile

(32) Shubin, V. E.; Kékicheff, P. *J. Colloid Interface Sci.* **1993**, *155*, 108.
(33) Senden, T. J.; Drummond, C. J. In preparation.

Figure 6. Force curves taken with the same colloid probe at pH 8.9 but for different electrolyte concentrations. The diffuse-layer potentials and the decay lengths both decrease with increasing salt as expected by theory. The fitting paramenters, determined with no Stern layer, for the three salt concentrations are as follows (the numbers in parentheses are the theoretical Debye lengths): (c) -38 mV, $\kappa^{-1} = 6.5$ nm (3.0 nm) at 1.0×10^{-2} M salt concentration, (b) -53 mV, $\kappa^{-1} = 10.0$ nm (10.1 nm) at 0.9×10^{-3} M salt concentration, and (a) -58 mV, $\kappa^{-1} = 30.0$ nm (30.4 nm) at 1.0×10^{-4} M salt concentration.

surfaces in aqueous solution. The figure also shows the theoretical force–separation curve given by eq 2 using a calculated Hamaker constant (see later).

In Figure 6 we show force–separation curves for various salt concentrations at pH 8.9. These measurements were taken with a different probe to that used in the pH study. As expected, both the diffuse-layer potential and the decay length decrease as the salt concentration is increased. There is excellent agreement between the decay length and the theoretical Debye length at low electrolyte concentrations, but at 10^{-2} M KNO_3 the decay length is greater than the Debye length. At the higher salt levels the measured force is considerably lower, and the signal-to-noise ratio is a lot lower than at low salt concentrations. Also, the extent of the surface force is comparable to the surface roughness. These may be the causes for the poorer agreement of experiment and theory at 10^{-2} M electrolyte. The jump-in distance for the probe used in the decay length study is less than that predicted by the DLVO theory. This variability is thought to be due to surface roughness effects.

It is also worth commenting that under the conditions studied (10^{-4} M KNO_3 as a function of pH, and 10^{-3} and 10^{-2} M KNO_3 at high pH) there is no evidence of a non-DLVO short range repulsive force that previous workers have reported in the cases of mica[34,35] and SiO_2.[1-3,29,30] Rutile TiO_2 is similar to sapphire (Al_2O_3) in this regard.[36] Other workers[37] have suggested the presence of this additional repulsive force at electrolyte concentrations higher than 2.0×10^{-2} M NaCl for TiO_2, based on turbidity data.

(iii) Calculation of the Non-retarded Hamaker Constant, A_H. The method described by Hough and White,[38] which employs the Ninham–Parsegian[39] representation of dielectric data, was used to calculate the value of the Hamaker constant using Lifshitz theory.[40] Dielectric data are used to construct the function ϵ-($i\xi$)—the dielectric constant at imaginary frequency $i\xi$. At $\xi = 0$, $\epsilon(0)$ is the static dielectric constant ϵ_{DC}. As ξ increases $\epsilon(i\xi)$

(34) Pashley, R. M. *J. Colloid Interface Sci.* **1981a**, *80*, 153.
(35) Pashley, R. M. *J. Colloid Interface Sci.* **1981b**, *83*, 531.
(36) Horn, R. G.; Clarke, D. R.; Clarkson, M. T. *J. Mater. Res.* **1988**, *3*, 413.
(37) Yotsumoto, H.; Yoon, R. *J. Colloid Interface Sci.* **1993**, *157*, 426.
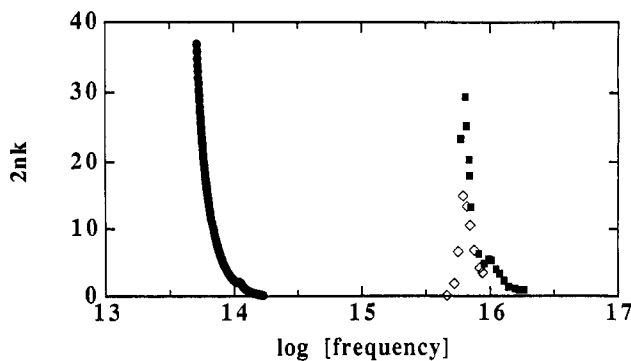(38) Hough, D. B.; White, L. R. *Adv. Colloid Interface Sci.* **1980**, *14*, 3.
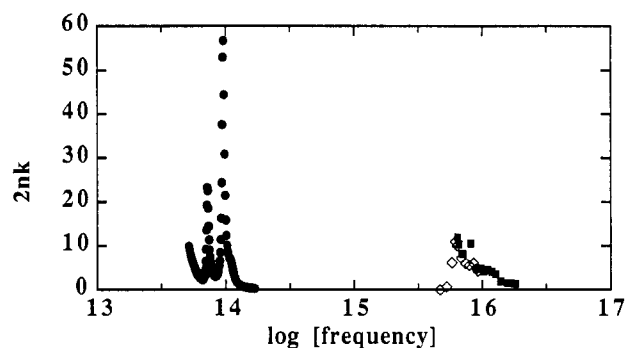(39) Ninham, B. W.; Parsegian, V. A. *J. Chem. Phys.* **1970**, *52*, 4578.
(40) Lifshitz, E. M. *Sov. Phys. JETP* **1956**, *2*, 73.

Figure 7. Absorption spectrum for the parallel orientation of the electric field to the crystal. On the y axis n is the refractive index and k is the absorption coefficient of the material at that frequency. The symbols refer to the different sources: (●) ref 52, (■) ref 53, (◊) ref 54.

Figure 8. Absorption spectrum in the perpendicular direction of the electric field to the crystal. On the y axis n is the refractive index and k is the absorption coefficient of the material at that frequency. The IR absorption band is at a higher frequency than in the parallel case and is therefore of greater importance in calculating the Hamaker constant. The area under the UV band is approximately 100 times greater than that under the band in the IR. The symbols refer to the different sources: (●) ref 52, (■) ref 53, (◊) ref 54.

is real and decreases toward 1 as $x \to \infty$. For TiO₂ we use the representation

$$\epsilon(i\xi) = \epsilon_{DC} \quad \text{when } \xi = 0$$

$$\epsilon(i\xi) = 1 + \frac{C_{IR}}{1 + (\xi/\omega_{IR})^2} + \frac{C_{UV}}{1 + (\xi/\omega_{UV})^2} \quad \text{when } \xi > 0$$

where C_i is the oscillator strength and ω_i is the absorption frequency in the infrared (IR) and ultraviolet (UV) regions.

The TiO₂ used possesses a tetragonal crystal structure which has uniaxial crystal symmetry. As a consequence the dielectric constant has different values in the directions parallel (∥) and perpendicular (⊥) to the c axis of the crystal. In Figures 7 and 8 we show the absorption spectra for rutile TiO₂ in the parallel and perpendicular orientations.[41] The data taken in the two different orientations had to be analyzed separately and, because of the two contributions in the perpendicular direction and only the one in the parallel direction, we used an average dielectric constant given by

$$\epsilon(i\xi) = {}^2/_3\epsilon_\perp(i\xi) + {}^1/_3\epsilon_\parallel(i\xi) \tag{5}$$

In this approach for calculating the Hamaker constant the function $\epsilon(i\xi)$ is sampled at frequency steps of $\approx 2.4 \times 10^{14}$ rad s⁻¹. Therefore there are many more sampling points in the UV region of $\epsilon(i\xi)$, and consequently this region has a greater importance in calculating Hamaker constants than the microwave and infrared regions.

(41) Ribarsky, M. W. *Handbook of Optical Constants of Solids*, Palik, E. Ed.; Academic Press, Inc.: New York, 1985; p 795.
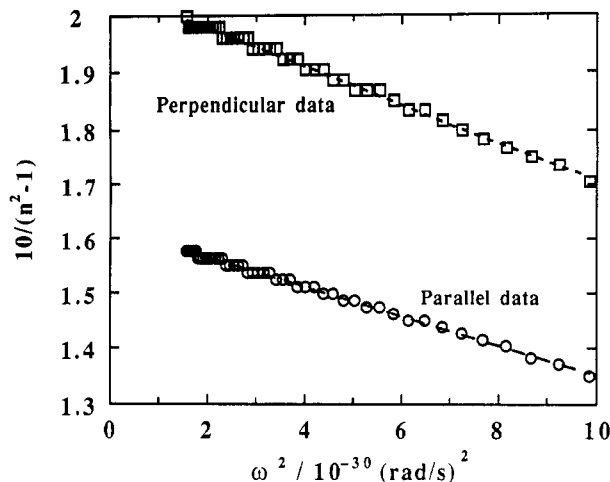
Figure 9. Cauchy plot for the data in the UV region of the absorption spectrum of rutile. The intercepts and slopes of the linear fits to the data are used to calculate the oscillator strengths and relaxation frequencies for the two orientations. n is the refractive index of the material at that frequency (frequency is in rad s⁻¹ as in the absorption spectra). The correlation coefficients are 0.998 for the parallel data and 0.997 for the perpendicular data.

The more important parameters in calculating the Hamaker constant are the oscillator strength, C_{UV}, and the relaxation frequency, ω_{UV}. The best available[37] ultraviolet optical data, shown in Figures 7 and 8, are inadequate for the purpose of determining the ultraviolet part of the $\epsilon(i\xi)$ construction. Effective C_{UV} and ω_{UV} parameters can, however, be obtained from a Cauchy plot of refractive index data in the visible region.[38] The Cauchy plot for the perpendicular and parallel orientations is shown in Figure 9. There are no significant absorptions in the microwave region[42–44] so the oscillator strength in the IR region can be worked out from

$$C_{IR} = \epsilon(0) - C_{UV} - 1 \tag{6}$$

The value of ω_{IR} lies between 5×10^{13} and 2×10^{14} rad s⁻¹, with the most probably value being 1×10^{14} rad s⁻¹.[43,44] These values along with the static dielectric constants for rutile were used to calculate the Hamaker constant. We also need to construct the function $\epsilon(i\xi)$ for water when it is the intervening medium. We used both the Gingell–Parsegian[45] and the newer Parsegian–Weiss[46] representations for water, the difference between the results using the two representations was negligible, see Table I. We did not interpolate into the far ultraviolet region. In Table I we show the calculated values of C_i and ω_i and values of the Hamaker constant with different intervening media. On the basis of these calculations, the Hamaker constant for rutile TiO₂ surfaces separated by water is $7 \pm 1 \times 10^{-20}$ J. Several experimental and theoretical values for the non-retarded Hamaker constant of rutile have been reported in the literature.[42,47–51] Recently, Buscall calculated a non-retarded Hamaker constant of $6.4 \pm 0.4 \times 10^{-20}$ J for rutile surfaces interacting across water.[42] Buscall's values are slightly lower than those presented in Table II primarily because he chooses a slightly lower value for ω_{IR}.

(42) Buscall, R. *Colloid Surf. A* **1993**, *75*, 269.
(43) Cronemeyer, D. C. *Phys. Rev.* **1952**, *87*, 879.
(44) Liebisch, T; Rubens, H. *Sitzungsber. Preuss. Akad. Wiss. Phys.-Math. Kl.* **1921**, 211.
(45) Gingell, D.; Parsegian, V. A. *J. Theor. Biol.* **1972**, *36*, 41.
(46) Parsegian, V. A.; Weiss, G. H. *J. Colloid Interface Sci.* **1981**, *81*, 285.
(47) Choudbury, B. K. *Nature* **1960**, *185*, 308.
(48) Fowkes, F. M. *Surfaces and Interfaces*, Syracuse University Press: New York, 1967; Vol. 1, p 199.
(49) Crowl, V. T. *J. Oil Colour Chem. Assoc.* **1967**, *50*, 1023.
(50) Parfitt, G. D. *Tenside* **1971**, *8*, 136.
(51) Israelachvili, J. N. *Intermolecular and Surface Forces, 2nd ed.*; Academic: London, 1991; p 191.
(52) Gervais, F.; Piriou, B. *Phys. Rev. B* **1974**, *10*, 1642.
(53) Cardona, M.; Harbeke, G. *Phys. Rev.* **1965**, *137A*, 1467.

Table I. Spectroscopic Parameters Used in the Calculation of the Non-retarded Hamaker Constant for Rutile TiO_2[a]

direction	$\epsilon(0)$	ω_{IR} (rad/s)	C_{IR}	ω_{UV} (rad/s)	C_{UV}	$\epsilon(i\zeta)$ ($\times 10^{20}$ J) (intervening medium)		
						(G–P water)	(P–W water)	(vacuum)
perpendicular	86	5×10^{13}	80	7.49×10^{15}	4.77	5.54	5.56	14.5
		1×10^{14}	80	7.49×10^{15}	4.77	5.95	5.97	14.9
		2×10^{14}	80	7.49×10^{15}	4.77	6.82	6.84	15.7
parallel	170	5×10^{13}	163	7.24×10^{15}	6.01	7.74	7.73	17.4
		1×10^{14}	163	7.24×10^{15}	6.01	8.31	8.30	18.0
		2×10^{14}	163	7.24×10^{15}	6.01	9.48	9.47	19.0

[a] Orientation refers to the direction of the radiation of the applied electric field and $\epsilon(0)$ is the static dielectric constant.[b] C_i and ω_i are the oscillator strengths and absorption frequencies, respectively. G–P water refers to calculations made with the Gingell–Parsegian representation of water as the intervening medium and P–W water refers to the Parsegian–Weiss representation. [b] *CRC Handbook of Chemistry and Physics*, 62nd ed.; CRC Press, Inc.: Boca Raton, FL, 1981–1982.

Table II. Values of the Non-retarded Hamaker Constant Using the Data Presented in Table I

w_{IR} (rad/s)	A_H ($\times 10^{20}$ J) (intervening medium)		
	(G–P water)	(P–W water)	(vacuum)
5×10^{13}	6.27	6.28	15.5
1×10^{14}	6.74	6.75	15.9
2×10^{14}	7.71	7.72	16.8

The comparison between the theoretical non-retarded van der Waals interaction and the experimental data is shown in Figure 5. The agreement may be partly fortuitous because at the separations where the attraction is measured one would expect retardation to influence the interaction.

Conclusions

An atomic force microscope has been successfully used to measure the forces between macroscopic TiO_2 surfaces as a function of separation distance, pH, and electrolyte concentration. An experimental non-retarded Hamaker constant of $6 \pm 2 \times 10^{-20}$ J was determined at the pH_{iep} of the TiO_2. This value is

(54) Vos, K.; Krusemeyer, H. J. *J. Phys. Chem.* **1977**, *10*, 3893.

comparable to a value of $7 \pm 1 \times 10^{-20}$ J calculated from available spectroscopic data on rutile TiO_2 using a method based on Lifshitz theory.